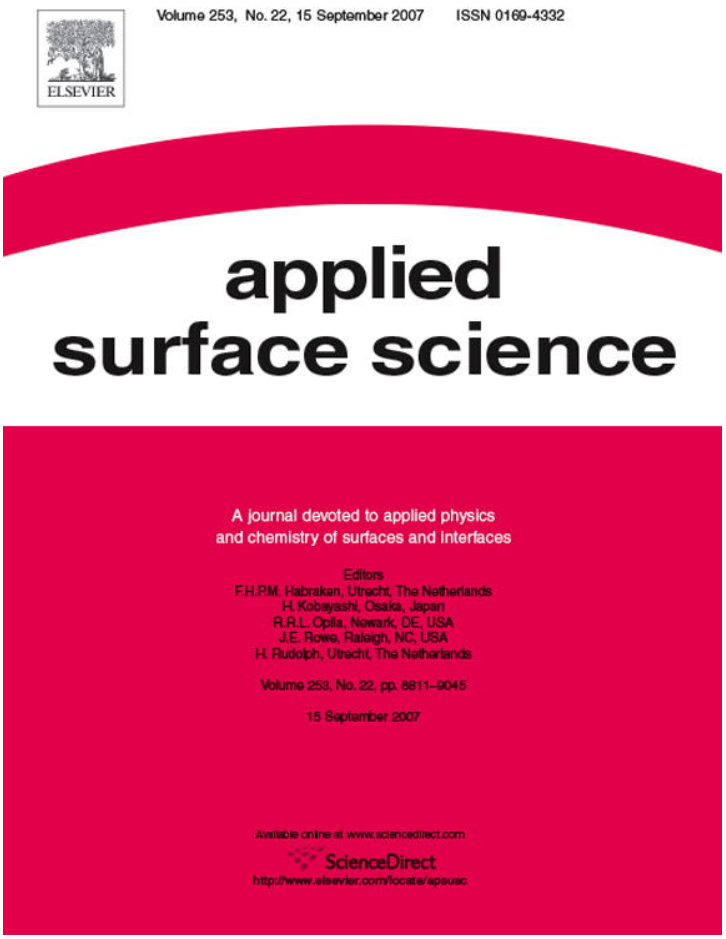

Available online at www.sciencedirect.com
ScienceDirect
Applied Surface Science 253 (2007) 8874–8878
applied surface science
www.elsevier.com/locate/apsusc

Surface ablation of lithium tantalate by femtosecond laser

Yishuai Zhang, Xianfeng Chen *, Hongyun Chen, Yuxing Xia

Department of Physics, the State Key Laboratory on Fiber Optic Local Area Communication Networks and Advanced Optical Communication Systems, Shanghai Jiao Tong University, Shanghai 200240, China

Received 2 April 2007; received in revised form 18 April 2007; accepted 26 April 2007
Available online 22 May 2007

Abstract

We report measurements of the laser induced breakdown threshold in lithium tantalate with different number of pulses delivered from a chirped pulse amplification Ti: sapphire system. The threshold fluences were determined from the relation between the diameter D^2 of the ablated area and the laser fluence F_0. The threshold of lithium tantalite under single-shot is found to be 1.84 J/cm^2, and the avalanche rate was determined to be 1.01 cm^2/J by calculation. We found that avalanche dominates the ablation process, while photoionization serves as a free electron provider.

Keywords: Laser ablation; Femtosecond laser; Lithium tantalate

1. Introduction

There is increasing interest in ultrashort pulse laser since its advent. Because of the high peak power, ultrashort pulse laser is widely used in micromachining of optical materials, high-density data storage, and biomedical technologies [1–7]. However, the high peak power will cause permanent damage to the material, which limits the development of these applications because it can prevent the transmission and deposition of energy in the transparent material. The first experiment to investigate the ultrashort-pulse laser damage was performed by Du et al. [8] in 1994. They reported two remarkable features of this kind of damage. First, opposite to long pulse damage, short-pulse damage exhibits some deterministic nature. Second, the damage threshold fluence deviates from the $\sqrt{\tau}$ scaling rule, where τ is the pulse duration. After that, many experimental and theoretical studies have been conducted to investigate the mechanism of ultrashort pulse-induced damage [9–13], and the thresholds of several materials have been determined [14,15].

Lithium tantalate (LT), the second member of the lithium-niobate family, has a large optical nonlinearity, high melting temperature, long storage time, and a wide band gap. In the past years, LT has been attracting more attentions, especially, periodically poled LT has been used as an efficient frequency conversion device. However, very little attention has been paid when it is irradiated by femtosecond laser with high peak power. In this paper, we study the surface ablation of LT using femtosecond pulsed laser beam, the information of damage threshold and ionization process are useful for its applications in frequency conversion and micromachine by femtosecond laser.

2. Experimental setup

For our damage testing, a chirped pulse amplification (CPA) Ti: sapphire system from Spectral Physics Corp. is used. The laser source delivers a train of pulses of 0.8 mJ at 800 nm with duration of 80 fs (FWHM), and a repetition rate of 1 kHz. Laser pulse energies were varied using a rotatable half-wave plate followed by a polarizer. The polarizer ensures that each pulse that arrives at the surface of the LT film has the same polarization. The attenuated pulses then passed through a speed-controllable shutter, which was used to control the number of pulses per spot. Finally the linearly polarized laser pulses were focused on the front surface of the LT to a $1/e^2$ diameter of $\approx$25 μm with a lens whose focal length is 50 mm, and the Rayleigh length is $\sim$2.4 mm. The target was positioned in the way that its surface was perpendicular to the direction of the incident laser beam. Fig. 1 gives a simplified picture of the experimental setup.

In our experiment, the incident laser beam has a Gaussian spatial profile with a $1/e^2$-beam radius ω_0, and we can obtain the

* Corresponding author.
E-mail address: xfchen@sjtu.edu.cn (X. Chen).

0169-4332/$ – see front matter
doi:10.1016/j.apsusc.2007.04.086

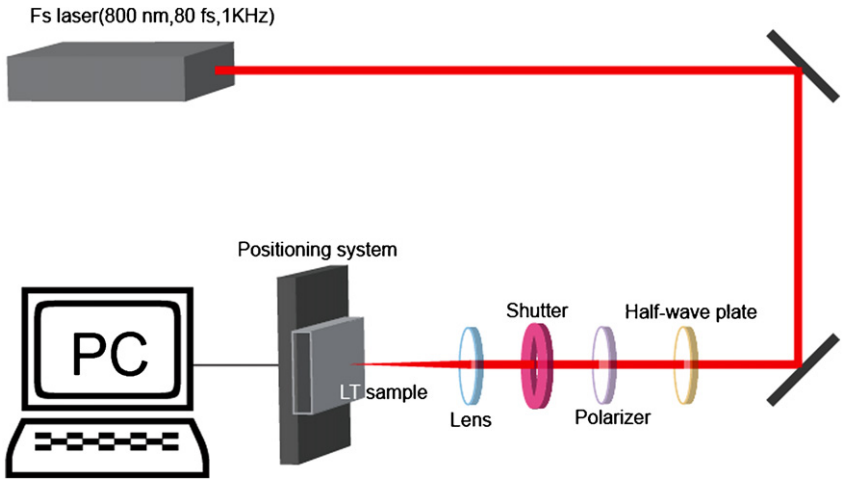

Fig. 1. Schematic of the experimental setup.

maximum laser fluence F_0 at the front surface of the sample through the following relation:

$$F_0 = \frac{2E_{\text{pulse}}}{\pi\omega_0^2}, \tag{1}$$

where E_{pulse} is the energy of each pulse. The spatial distribution of laser fluence has a Gaussian shape, and can be written as

$$F(x) = F_0 \exp\left(-\frac{2x^2}{\omega_0^2}\right), \tag{2}$$

with the Gaussian beam radius ω_0. Suppose the diameter of the ablated area is D, then the laser threshold is $F(x = D/2)=F_{\text{th}}$. So we can obtain the relation between the diameter of the damaged area and the maximum laser fluence F_0:

$$D^2 = 2\omega_0^2 \ln\left(\frac{F_0}{F_{\text{th}}}\right) \tag{3}$$

If we can obtain a series of D under different pulse energies, then we can obtain the beam radius and the laser fluence.

3. Experimental results and discussions

A typical snapshot picture of the ablated area under single shot experiment, which was taken from a 400× microscope, is shown in Fig. 2(a). In this case, the peak intensity of the pulse was 2.15×10^{14} W/cm^2. The shape of the ablated area is not perfectly round, this may be due to the fact that the spatial distribution of the incident pulse was not ideally Gaussian-profile, and the LT crystal itself is anisotropic, as has been reported in Ref. [16]. By contrast, Fig. 2(b) shows the ablated area of the sample under 70 shots with the same energy of each pulse that used in the single-shot experiment. We can see that the damage created by the multishot is larger on the surface, and deeper into the sample (the center of the area is darker compared with that of single-shot).

Fig. 3 shows the measured fluence dependence of the squared diameter of the ablated area under single shot. According to Eq. (3), the slope of the fitted line gives some information of the beam radius of the input pulse, and we can obtain $\omega_0 = 25$ μm. By extrapolate the fitted line to $D^2 = 0$, the threshold is found to be $F_{\text{th}} = 1.84$ J/cm^2.

Multi-shot experiments were performed to provide some insight into the relation between single-shot threshold and that of multi-shot. A shutter was used to control the number of shots per spot. Part of the experimental result is given in Fig. 4. The spots form a matrix, those in the same horizontal line endured pulse beams with the same power, and those standing in the same vertical line suffered the same number of shots. Notice that the spots in the same vertical line grow in size from top to bottom, and this can also be explained by the Eq. (3), even if the equation is deduced from the single-shot model. A little increase in size

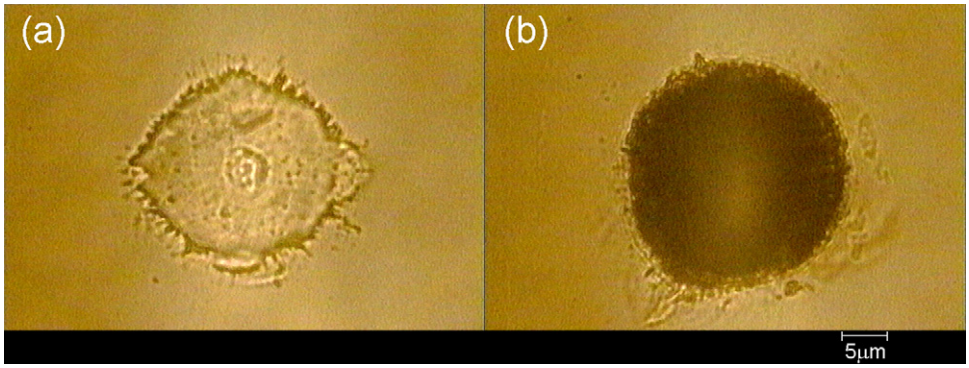

Fig. 2. (a) The micrograph of an ablated spot of the LT surface under single shot. (b) The micrograph of an ablated spot of the LT surface under 70 shots.

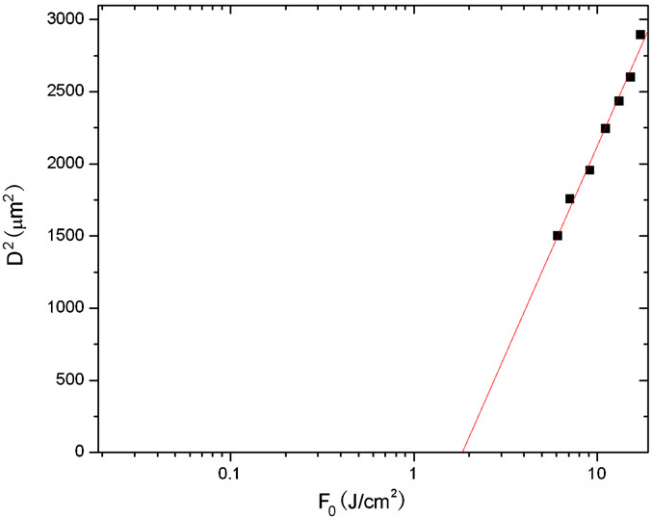

Fig. 3. Squared diameter (D^2) vs. laser fluence F_0 (single-shot).

can also be observed with spots in the same horizontal line. This observation hints that there may be some connections between thresholds of different number of shots [17].

Fig. 5 shows the results of single and multiple shots. Taking the error of measurements into consideration, the error of the fitted line using the same slope as that of single shot is acceptable, which could be explained as that Eq. (3) may still hold for the sample under multi-shot. But we would like to point out that this conclusion doesn't hold anymore when the sample undergoes more shots (not shown in Fig. 5). We find that when the number of shots exceeds 60, the results don't differ distinctly with each other. This may be due to the accumulative effect of each pulse's energy. Table 1 gives the threshold fluence of the sample under different number of shots, which were determined by Eq. (3).

Our results show that the threshold descends as the number of shots increases, this is also reported by recent studies on femtosecond ablation of doped and undoped lithium niobate crystals [18,19], and could be explained by the defect enhanced absorption [17,18]. In our study, it is found that the ablation threshold for lithium tantalite is smaller than that reported for lithium niobate. Further studies need to be carried out to have a good understanding of the result.

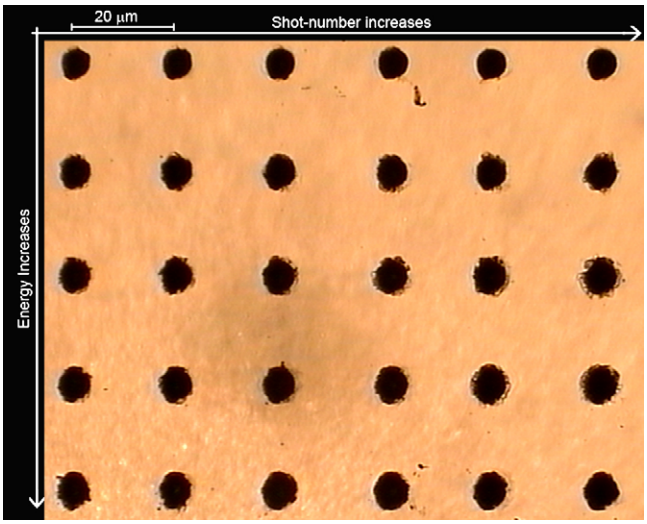

Fig. 4. The ablation matrix, power increases from top to bottom and shot-numbers increases from left to right.

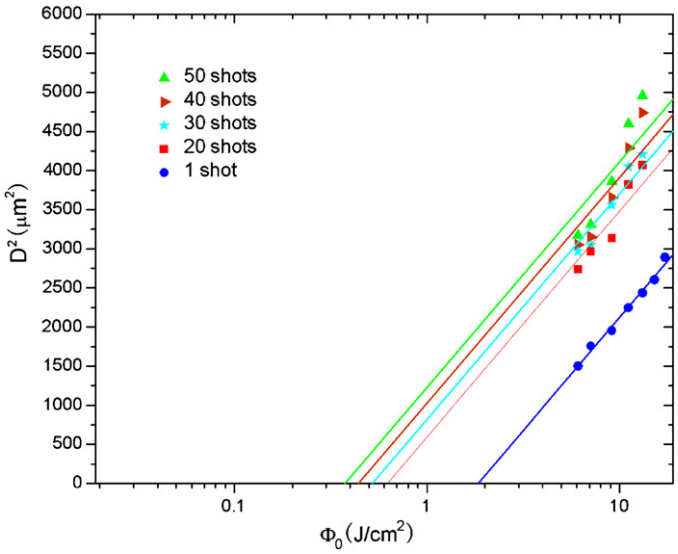

Fig. 5. Squared diameter of ablated area versus laser fluence.

Table 1
Pulse laser ablation of lithium tantalite film, 800 nm, linearly polarized, focused area 2.0×10^{-5} cm^2

Number of shots	Threshold fluence/Jcm^{-2}
1	1.840724
20	0.621878
30	0.521284
40	0.441053
50	0.375923

4. Theoretical model: calculation of avalanche rate

Generally speaking, the ablation of the material can be described in terms of three major progresses: (1) the excitation of electrons in the valued band to the conduction band, (2) energy absorption of the conduction-band electrons from the radiation and plasma formation, (3) transferring the energy from the plasma to the lattice. As the material becomes highly absorbing when the free electron density exceeds the critical plasma density (1.6×10^{21} cm^{-3} for a laser wavelength of 800 nm [8]), this critical plasma density is taken as the criterion of the onset of ablation.

In order to reveal when laser ablation occurred, a rate equation is commonly used to predict the evolution of the conduction-band electron density ρ [11,13,20]

$$\frac{d\rho}{dt} = (W_{PI}(E) + \eta(E)\rho)\left(1 - \frac{\rho}{\rho_{max}}\right) \quad (4)$$

where $\eta(E)$ is the electron avalanche rate, $W_{PI}(E)$ is the photoionization rate, and is a function of the electric field,

and ρ_{max} denotes the maximum density. In our calculation, Stuart's et al. [10] model was used, that is, $\eta(E)$ scales linearly with the laser intensity: $\eta(E) = \beta I(t)$, where β is the avalanche coefficient, and $I(t)$ is the intensity of the laser pulse. The recombination of electrons was simply neglected in our model because the characteristic time is larger than the pulse duration. As our incident laser beam has a Gaussian temporal profile, the focus point of the sample undergoes an electric field that varies with time. If $E(t)$ is known, the avalanche coefficient β can be calculated by Eq. (4). In Part 3, we already have obtained the value of the threshold fluence, and we have.

$$F_{th} = \int_{-\infty}^{+\infty} I_{th} \exp\left[-2.76 \left(\frac{t}{\tau_p} \right)^2 \right] dt \quad (5)$$

Eq. (5) shows the relationship between fluence threshold and laser intensity threshold, where I_{th} is the intensity threshold. The analytical value of I_{th} can be deduced from Eq. (5), and is given to be

$$I_{th} = \frac{\sqrt{2.76} \times F_{th}}{\tau_p \times \sqrt{\pi}} \quad (6)$$

and the relation between I_{th} and E_{th} is

$$I_{th} = \frac{n}{2c\mu_0} |E_{th}|^2, \quad (7)$$

where n is the refractive index, c is the speed of light in vacuum, μ_0 is the permeability of vacuum, and E_{th} is the maximum and threshold of electric field. Combining Eq. (6) with Eq. (7), we can work out E_{th} from the measured data F_{th}.

In order to get the photoionization rate $W_{PI}(E)$ in Eq. (4), we have used Keldysh's formulation [21]:

$$W_{PI}(E) = \frac{2\omega}{9\pi} \left(\frac{\omega m}{\hbar \sqrt{\gamma_1}} \right)^{3/2} Q(\gamma, x) \exp(-\alpha < x + 1 >), \quad (8)$$

where

$$\gamma_1 = \frac{\gamma^2}{1+\gamma^2}, \quad \gamma_2 = \frac{1}{1+\gamma^2},$$

$$Q(\gamma, x) = \sqrt{\frac{\pi}{2K(\gamma_2)}} \times \sum_{n=0}^{\infty} \exp(-n\alpha) \Phi(\sqrt{\beta(n+2\nu)}),$$

$$\alpha = \pi \frac{K(\gamma_1) - E(\gamma_1)}{E(\gamma_2)}, \quad \beta = \frac{\pi^2}{4K(\gamma_2)E(\gamma_2)},$$

$$x = \frac{2}{\pi} \frac{\Delta}{\hbar\omega} \frac{E(\gamma_2)}{\sqrt{\gamma_1}}, \quad \nu = < x + 1 > - x,$$

where $\gamma = \frac{\omega\sqrt{m\Delta}}{eE}$ is Keldysh's parameter, $\langle \bullet \rangle$ denotes the integer part, ω is the laser frequency, m is the reduced mass of the electron and the hole, $K(x)$ and $E(x)$ are complete elliptic integral of the first and second kinds, Δ is the energy gap of the material, and $\Phi(z) = \int_0^z \exp(y^2 - z^2) dy$ is the Dawson integration. In the case of low frequencies and strong fields, $\gamma \gg 1$, Eq. (8) describes the tunnel effect, if laser frequencies are high enough and the fields are week, $\gamma \ll 1$, Eq. (8) describes the multiphoton absorption effect. Fig. 6 gives the general trend of photoionization rate as a function of electric field, and the parameters used in calculation are showed in the figure. The figure is similar as those in Ref. [11,13,20].

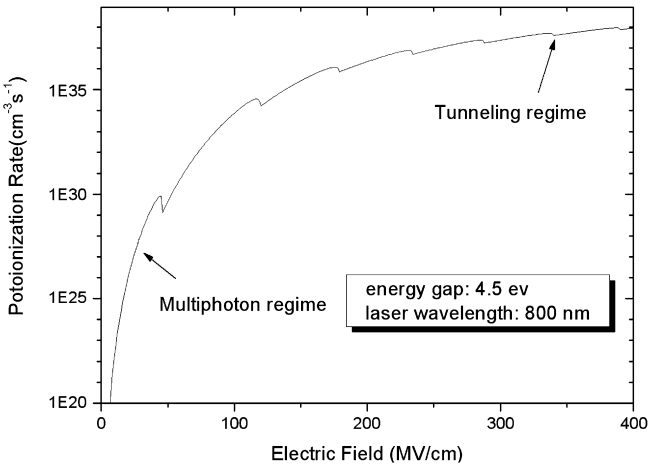

Fig. 6. Photoionization rate in LT as predicted by Keldysh's mode.

By using the value of single-shot threshold, the avalanche coefficient β can be predicted by postulating that the critical plasma density is achieved at the end of the pulse by Eq. (4). The parameters used in our simulation are listed in Table 2. Generally speaking, the calculation of a differential equation is sensitive to the initial values, but in our simulation, results calculated from different initial electron densities gave no difference. By calculation, we achieve the avalanche coefficient β to be 1.01 cm^2/J. This can be explained by Fig. 7, the dotted line in the figure shows the evolution of the electron density if

Table 2
Parameters used in the simulation

Symbol	Description	Value
λ_0	Laser wavelength	800 nm
ω_0	Beam radius at the focal point	25 μm
τ	Pulsewidth	80 fs
Δ	Band gap	4.5 eV [22]
m	Effective mass of electron	0.86 m_e [13]
n	Refractive index of LT	2.17337 [23]
ρ_{max}	Maximum electron density	1.90E22 cm^{-3}

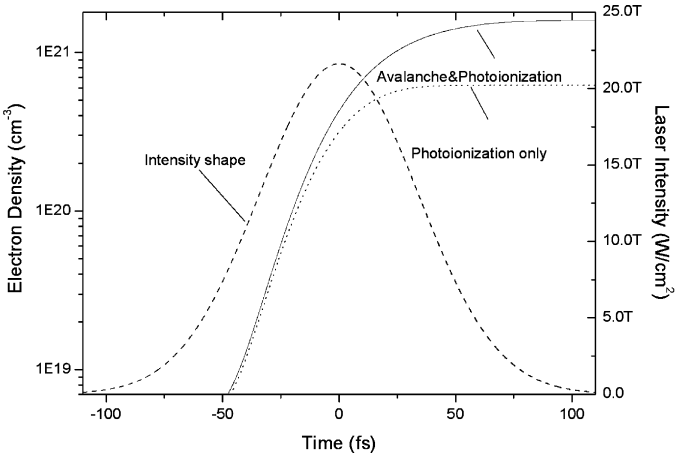

Fig. 7. Calculated electron density evolution of the conduction band for a 80 fs, 800 nm pulse.

only photoionization is taken into consideration, while the solid line gives the result of the condition that both photoionization and avalanche are considered. We can see that at the leading edge of the pulse, the electrons build up very fast in the conduction band mainly by the effect of photoionization, which leads the evolution. Then at some point near the center of the pulse, the density climbs up to some critical density, avalanche surpasses photoionazation, and starts to dominate the ablation process or the evolution of the electron density. Finally, at the end of the pulse, the density reaches critical plasma density, and ablation occurs. In this process, photoionazation serves as a seed electron supplier, and the initial electron density in the conduction band is neglectable. Our conclusions are in accordance with previous theoretical work [10,11].

5. Conclusion

In summary, surface ablation experiments with Ti: sapphire laser pulses on lithium tantalate were investigated. We measured the damage thresholds of lithium tantalate under different number of shots from the source. By calculation, we worked out the avalanche rate as large as 1.01 cm^2/J in the ablation process, and come to the conclusion that avalanche dominates the process, while photoionization serves as a free electron provider.

Acknowledgements

This research was supported by the National natural science foundation of China (No. 60477016 and No. 10574092), the National basic research program "973" of China (2006CB806000).

References

[1] E. Bricchi, B.G. Klappauf, P.G. Kazansky, Opt. Lett. 29 (2004) 119.
[2] D.G. Papazoglou, M.J. Loulakis, Opt. Lett 31 (2006) 1441.
[3] W. Perrie, A. Rushton, M. Gill, P. Fox, W. O'Neill, Appl. Surf. Sci. 248 (2005) 213.
[4] Y. Fu, T.-T. Han, Y. Luo, H. Ågren, Appl. Phys. Lett. 88 (2006) 221114.
[5] A.M. Kowalevicz, V. Sharma, E.P. Ippen, J.G. Fujimoto, K. Minoshima, Opt. Lett. 30 (2005) 1060.
[6] M. Nakano, Y. Kawata, Appl. Opt. 44 (2005) 5966.
[7] M.A.A. Neil, R. Juskaitis, M.J. Booth, T. Wilson, T. Tanaka, S. Kawata, Appl. Opt. 41 (2002) 1374.
[8] D. Du, X. Liu, G. Korn, J. Squier, G. Mourou, Appl. Phys. Lett. 64 (1994) 3071.
[9] M. Lenzner, J. Krüger, S. Sartania, Z. Cheng, Ch. Spielmann, G. Mourou, W. Kautek, F. Krausz, Phys. Rev. Lett. 80 (1998) 4076.
[10] B.C. Stuart, M.D. Feit, A.M. Rubenchik, B.W. Shore, M.D. Perry, Phys. Rev. Lett. 74 (1995) 2248.
[11] A.-C. Tien, S. Backus, H. Kapteyn, M. Murnane, G. Mourou, Phys. Rev. Lett. 82 (1999) 3883.
[12] J. Ren, M. Kelly, L. Hesselink, Opt. Lett. 30 (2005) 1740.
[13] A.Q. Wu, I.H. Chowdhury, X.F. Xu, Phys. Rev. B 72 (2005) 085128.
[14] W. Kauteka, J. Krüger, M. Lenzner, S. Sartania, C. Spielmann, F. Krausz, Appl. Phys. Lett. 69 (1994) 3146.
[15] D. Ashkenasi, M. Lorenz, R. Stoian, A. Rosenfeld, Appl. Surf. Sci. 150 (1999) 101.
[16] G. Zhou, M. Gu, Appl. Phys. Lett. 87 (2005) 241107.
[17] A.B. Yakar, R.L. Byer, J. Appl. Phys. 96 (2004) 5316.
[18] D.C. Deshpande, A.P. Malshe, E.A. Stach, V. Radmilovic, D. Alexander, D. Doerr, D. Hirt, J. Appl. Phys. 97 (2005) 074316.
[19] A. Ródenas, J.A.S. García, D. Jaque, G.A. Torchia, C. Mendez, I. Arias, L. Roso, F.A. Rueda, J. Appl. Phys. 100 (2006) 033521.
[20] A. Couairon, L. Sudrie, M. Franco, B. Prade, A. Mysyrowicz, Phys. Rev. B 71 (2005) 125435.
[21] L.V. Keldysh, Sov. Phys. JETP. 20 (1965) 1018.
[22] S. Chao, C.-C. Hung, Appl. Phys. Lett. 69 (1996) 3803.
[23] W. Xie, X.F. Chen, Y.P. Chen, Y.X. Xia, Chin. Opt. Lett. 2 (2004) 664.